# Electrostatic potentials for metal-oxide surfaces and interfaces

F. H. Streitz and J. W. Mintmire
*Code 6179, U.S. Naval Research Laboratory, Washington, D.C. 20375-5342*
(Received 10 May 1994)

As most technologically important metals will form oxides readily, any complete study of adhesion at real metal surfaces must include the metal-oxide interface. The role of this ubiquitous oxide layer cannot be overlooked, as the adhesive properties of the oxide or oxide-metal system can be expected to differ profoundly from the adhesive properties of a bare metal surface. We report on the development of a computational method for molecular-dynamics simulations, which explicitly includes variable charge transfer between anions and cations. This method is found to be capable of describing the elastic properties, surface energies, and surface relaxation of crystalline metal oxides accurately. We discuss in detail results using this method for $\alpha$-alumina and several of its low-index faces.

## INTRODUCTION

Many ceramic and metal properties are critically dependent on the underlying properties of internal metal-ceramic and ceramic-ceramic interfaces. A range of technologically important materials applications are affected by the properties of these interfaces: ceramic-metal composite materials, metal support in catalysis, conductive metals on metal-oxide substrates in electronic devices, and protective surface-oxide layers on structural metals are just a few representative examples. The atomistic structure of these interfaces is expected to influence strongly such macroscopic properties as the elastic response, electrical properties, and diffusion and segregation along the interface. Experimentally, the determination of the atomic structure at a buried interface is difficult, if not impossible. Because metal oxides are an important class of ceramic materials, atomic-scale simulations of metal-oxide materials and metal-oxide interfaces are an important tool for understanding and predicting the effect of the interface region on materials properties. Such simulations are difficult, however, both at the first-principles level and at the empirical level. For first-principles methods, the unit-cell sizes—particularly for defect supercell simulations—tend to be large, increasing the computational requirements of the simulation. Empirical potentials for these materials are also difficult because of the complexity of the bonding interactions in metal–metal-oxide systems.

One primary objective we have in our current research is to simulate the atomic-scale dynamics and energetics of technologically important metal–metal-oxide interfaces. To do this we need an empirical method that allows the local cation valence to vary according to the local environment and which includes the Coulombic electrostatic interaction among the anions and cations. An extensive literature of modeling local atomic charge for organic and biological systems based on long-range electrostatic interactions and local atomic electronegativity-based properties has developed over the last several decades.[1–6] We have developed a model based on this approach for a direct calculation of charge transfer in metal-oxide systems and incorporated the resulting electrostatic potential into an overall model potential for the $\alpha$-alumina system.

An important first step for simulating the interface correctly is to describe the bare surfaces well. The work described herein discusses our current work for the $\alpha$-alumina system. We present below our approach for modeling the electrostatic component of the potential energy of ionic systems, the electrostatic plus (ES+) method, and how standard empirical potential techniques can be effectively merged with this approach. We then discuss our results for both crystalline $\alpha$-alumina and several of its low-index faces. We compare these initial results with both extant experimental results, where available, and first-principles theoretical simulations otherwise. Our results indicate that this approach can provide physically realistic empirical potentials for future simulations on mixed metal–metal-oxide systems.

## METHODS

One of the dominant interactions in the metal oxides is the Coulombic electrostatic interaction between anions and cations. Earlier models using empirical potentials[7–9] included such effects by incorporating fixed atomic charges and polarizability functions into the energetics of metal oxides. Consider, however, a heterogeneous electrostatic environment, such as the interface between a metal and a metal oxide. The picture of fixed ionic charges situated on atomic nuclei is clearly incorrect here, as the charge or valence state of the metal atom must vary from zero (in the metal bulk) to near fully ionic (in the oxide bulk). Because our ultimate goal in this work is to develop relatively simple empirical potentials for studying precisely this type of interface, we have included an ability to calculate the local atomic charge (or equivalently, the valence) based on the local environment of each atom. This capability is lacking in earlier empirical approaches. As the Coulomb interaction is very long ranged, the spatial dimensions of this *local* environment will be relatively large scale, of the dimensions of the screening length in metal oxides.

0163-1829/94/50(16)/11996(8)/$06.00  

### The ES+ approach

Conceptually then, what is needed is a description of the total electrostatic energy of an array of atoms as a function of atomic charges (valences) and position. Consider expanding the energy of a neutral atom $i$ as a Taylor series in the partial charge, $q_i$. The first derivative term $\partial E/\partial q_i$ is traditionally denoted as the electronegativity.[1,2] The second derivative term has been associated with an atomic hardness[3] or with a self-Coulomb repulsion.[6] Using the notation of Rappé and Goddard,[6] the local atomic energy $E_i(q_i)$ can be expressed to second order as $E_i(q_i)=E_i(0)+\chi_i^0 q_i+\frac{1}{2}J_i^0 q_i^2$.

The electrostatic energy $E_{\rm es}$ of a set of interacting atoms with total atomic charges $q_i$ is then given by the sum of the atomic energies $E_i$, and the electrostatic interaction energies between all pairs of atoms,

$$E_{\rm es}=\sum_i E_i(q_i)+\frac{1}{2}\sum_{i\neq j} V_{ij}(\mathbf{r}_{ij};q_i,q_j) \ . \tag{1}$$

The Coulomb pair interaction $V_{ij}(\mathbf{r}_{ij};q_i,q_j)$ is given by the electrostatic interaction

$$V_{ij}(\mathbf{r}_{ij};q_i,q_j)=\int d^3r_1\int d^3r_2\rho_i(\mathbf{r}_1;q_i)\rho_j(\mathbf{r}_2;q_j)/r_{12} \ , \tag{2}$$

where $\rho_i(\mathbf{r};q_i)$ is the charge distribution about atom $i$ (including the nuclear point charge) for total charge $q_i$. The simplest model for $\rho_i(\mathbf{r};q_i)$ is as a point charge of charge $q_i$; this leads to $V_{ij}(\mathbf{r}_{ij};q_i,q_j)=q_iq_j/r_{ij}$. Rappé and Goddard[6] have suggested the use of spherically symmetric Slater-type orbitals to generate a $\rho_i(\mathbf{r};q_i)$ linear in $q_i$. For the work herein, we assume an atomic-charge-density distribution of the form

$$\rho_i(\mathbf{r};q_i)=Z_i\delta(\mathbf{r}-\mathbf{r}_i)+(q_i-Z_i)f_i(\mathbf{r}-\mathbf{r}_i) \ , \tag{3}$$

where $Z_i$ is an effective core charge which should satisfy the condition $0<Z_i<Z_i$, with $Z_i$ the total nuclear charge of the atom. The function $f_i$ describes the radial distribution of the valence charge in space.

Applying Eqs. (2) and (3) we find that

$$E_{\rm es}=\sum_i E_i(q_i)+\frac{1}{2}\sum_{i\neq j}\{q_iq_j[f_i|f_j]+q_iZ_j([j|f_i]-[f_i|f_j])+q_jZ_i([i|f_j]-[f_i|f_j])$$
$$+Z_iZ_j([f_i|f_j]-[i|f_i]-[j|f_i]+1/r_{ij})\} \ . \tag{4}$$

The notation $[\rho_a|\rho_b]$ denotes a Coulomb interaction integral between the charge densities $\rho_a$ and $\rho_b$,

$$[\rho_a|\rho_b]=\int d^3r_1\int d^3r_2\frac{\rho_a(\mathbf{r}_1)\rho_b(\mathbf{r}_2)}{r_{12}} \ , \tag{5}$$

and the $[a|\rho_b]$ notation denotes a nuclear-attraction integral,

$$[a|\rho_b]=\int d^3r\frac{\rho_a(\mathbf{r})}{|\mathbf{r}-\mathbf{r}_a|} \ . \tag{6}$$

For simplicity, we model the atomic-density distribution as a simple exponential of the form $f_i(|\mathbf{r}-\mathbf{r}_i|)=(\zeta_i^3/\pi)\exp(-2\zeta_i|\mathbf{r}-\mathbf{r}_i|)$, where $\mathbf{r}_i$ is the location of atom $i$ and $\mathbf{r}$ is a vector in space. (This distribution could be constructed from Slater $1s$ orbitals.) The choice of form for $f_i$ was made entirely for mathematical convenience; the entire model could be formulated with a more complicated (and perhaps more realistic) distribution function which is nonspherical (e.g., constructed from $p$ or $d$ orbitals). Such a choice would not only allow a directional dependence to the bonds but would introduce, for instance, local polarizability in a very natural way. Although we have not yet included such extensions, we feel that they remain promising avenues for the simulation of less ionic materials, where directionality will play a larger role.[10]

We can apply the above equations to yield an expression for the electrostatic energy:

$$E_{\rm es}=E_0+\sum_i q_i\chi_i+\frac{1}{2}\sum_{i,j} q_iq_jV_{ij} \ , \tag{7}$$

where

$$E_0=\sum_i E_i(0)+\frac{1}{2}\sum_{i\neq j} Z_iZ_j([f_i|f_j]-[i|f_j]$$
$$-[j|f_i]+1/r_{ij}) \ , \tag{8}$$

$$\chi_i=\chi_i^0+\sum_j Z_j([j|f_i]-[f_i|f_j]) \ , \tag{9}$$

$$V_{ij}=J_i^0\delta_{ij}+[f_i|f_j] \ . \tag{10}$$

Note that $E_0$ in Eq. (8) is strictly dependent on nuclear coordinates with no dependence on the atomic charges $q_i$. It thus behaves as a sum of pair potentials. We will later model the residual interatomic potential with an embedded-atom model that includes interatomic pair potentials. For computational simplicity we therefore treat $E_0$ as implicitly included in these other pair potentials and exclude it from the electrostatic energy without loss of generality. Similarly, we neglect one-center terms of the form $[f_i|f_i]$. (They would merely introduce a constant term to $\chi_i$ and $V_{ij}$, which would make $\chi_i^0$ and $J_i^0$ unnecessarily dependent on the choice of $\zeta_i$.)

For crystalline systems we can modify molecular-scale techniques straightforwardly to accommodate the periodicity and infinite size of the lattice. First, we choose the sum of atomic charges $\sum_i q_i=0$ to enforce net-charge neutrality and avoid any divergent behavior in the electrostatic potential. Second, we must modify Eqs. (9) and (10) to account for the crystalline periodicity. Letting the notation $f_i^{\mathbf{R}}$ denote the distribution $f_i(\mathbf{r}_i-\mathbf{R})$, we can rewrite expressions for $\chi_i$ and $V_{ij}$:

$$\chi_i=\chi_i^0+\sum_j Z_j\left\{\sum_{\mathbf{R}}([j|f_i^{\mathbf{R}}]-[f_i^0|f_j^{\mathbf{R}}])\right\}, \tag{9'}$$

$$V_{ij}=J_i^0\delta_{ij}+\sum_{\mathbf{R}}[f_i^0|f_j^{\mathbf{R}}], \tag{10'}$$

where $\mathbf{R}$ is a periodic translation of the unit cell in space.

Two-center Coulomb integrals such as $[f_i|f_j]$ and $[i|f_j]$ have been well studied in the literature.[11,12] Our choice of exponential-based distributions leads to these integrals decomposing into a leading $1/r_{ij}$ term and additional terms exponentially decaying as a function of $r_{ij}$. For computational convenience we thus decompose all the resulting lattice sums into those involving $1/r_{ij}$ terms and those involving exponentially damped terms. The long-range $1/r_{ij}$ terms cancel from $\chi_i$ in Eqs. (9) and (9'), above, leaving only the $1/r_{ij}$ term in $V_{ij}$. We evaluate this lone term using standard Ewald techniques;[13–18] the short-range terms we evaluate by direct summation.

For well-behaved parameters $J_i^0$ and functions $f_i(\mathbf{r})$, the electrostatic energy will have a well-defined minimum. We thus choose the values of $q_i$ as those that minimize $E_{\rm es}$ subject to the constraint that the sum of the $q_i$ be constant. This condition is, of course, algebraically equivalent to the electronegativity equalization condition[4–6] that the chemical potentials $\mu=\mu_i\equiv\partial E_{\rm es}/\partial q_i$ be equal. This leads to the condition

$$\sum_j V_{ij}q_j=\mu-\chi_i\ . \tag{11}$$

Defining $V_{ij}^{-1}$ to be the matrix inverse of $V_{ij}$, we find that

$$q_i=\sum_j V_{ij}^{-1}(\mu-\chi_j)\ ,$$
$$\mu=\left[\sum_{i,j}V_{ij}^{-1}\chi_j\right]\Big/\left[\sum_{i,j}V_{ij}^{-1}\right]\ . \tag{12}$$

### Implementation of ES+ embedded-atom method

The electrostatic energy is just one component of the total energy of a metal-oxide (or metal) system. Indeed, the electrostatic interaction between cations and anions will be strictly attractive at any internuclear separation, so that in the short-range limit a repulsive potential will be needed to maintain physically reasonable internuclear separations. As a first step in developing a total empirical potential for metal oxides, we originally expressed the total energy $E(\mathbf{r}_1,\mathbf{r}_2,\ldots)$ as a sum of the electrostatic energy $E_{\rm es}$ and pair-pair interaction energies.[19,20] We found, however, that the use of strictly pair-wise potentials for the nonelectrostatic interactions could lead to unphysical behavior near oxide surfaces. (The average coordination of atoms at or near a surface is reduced from that in bulk, which typically results in a local increase in bond strength. As pair potentials are insensitive to changes in coordination, surface atoms interacting with pair potentials are typically too weakly bound. In a partially ionic compound, such as an oxide, the electrostatics at such a surface dominate, resulting in unphysical relaxations and instabilities.)

We could without loss of generality replace the sum of pair potentials with any standard empirical potential which is a function of the nuclear positions, such as an embedded-atom method (EAM) approach,[21–26] or a many-body potential such as that developed by Abell and others for covalent systems.[27–31] We discuss here the merging of this model with an EAM approach. We chose the EAM scheme in large part because it is a commonly accepted and widely used technique for modeling metallic bonding.

We assume, then, that the total energy is given as the sum of the electrostatic energy $E_{\rm es}$ defined above and an EAM potential energy with the standard form

$$E_{\rm EAM}=\sum_i F_i[\rho_i]+\sum_{i<j}\phi_{ij}(r_{ij}) \tag{13}$$

with $F_i[\rho_i]$ the energy required to embed atom $i$ in a local electron density $\rho_i$ and $\phi_{ij}(r_{ij})$ the residual pair-pair interactions, with $r_{ij}$ the interatomic distance between atoms $i$ and $j$. For mathematical convenience, we have chosen the Finnis-Sinclair[24] form of the embedding energy,

$$F_i[\rho_i]=-A_i\sqrt{\rho_i/\xi_i}\ . \tag{14}$$

The local atomic density $\rho_i$ is given as the linear superpositions of the atomic density functions for all other atoms. These densities are well represented by exponential functions:

$$\rho_i(\mathbf{r})=\sum_{j\neq i}\xi_j\exp[-\beta_j(r_{ij}-r_j^*)]\ . \tag{15}$$

The pair potentials $\phi_{ij}(r)$ are defined uniquely for each unique combination of atom types, and are chosen to be of the form

$$\phi_{ij}(r)=2B_{ij}\exp\left[-\frac{\beta_{ij}}{2}(r-r_{ij}^*)\right]$$
$$-C_{ij}[1+\alpha(r-r_{ij}^*)]\exp[-\alpha(r-r_{ij}^*)]\ . \tag{16}$$

The form of $\phi_{ij}$ was motivated by a desire that the total energy of the system should behave as the universal equation of state plus an electrostatic term. The binding energy of virtually all solids has been shown to scale with length according to a universal function, which can be well presented by a simple Rydberg function.[32,33] This analysis has been extended to show that even ionic diatomic molecules could be described with a universal energy function if one adds explicitly the electrostatic or Coulomb term.[34,35] Using the ES+ model, the total energy of an oxide cannot be described as simply as can a diatomic molecule, making the "universality" of the total energy difficult to enforce. Consider, however, the total energy of a monoatomic system with interactions restricted to nearest neighbors. The function $\rho$ becomes simply $\rho=N\xi\exp[-\beta(R-r^*)]$, where $N$ is the number of nearest neighbors and $R$ is the equilibrium nearest-neighbor distance. Equation (13) can be written

$$E_{\mathrm{EAM}}^{\mathrm{nn}}=NF[\rho]+\frac{N}{2}\phi(R)$$
$$=-NA\sqrt{N}\exp\left[-\frac{\beta}{2}(R-r^*)\right]+\frac{N}{2}\phi(R)\ . \tag{17}$$

If we require that the total energy behaves as a Rydberg function,

$$E_{\mathrm{EAM}}^{\mathrm{nn}}=-NE_c[1+\alpha(R-r^*)]\exp[-\alpha(R-r^*)]\ ,$$

then

$$\phi(R)=2A\sqrt{N}\exp\left[-\frac{\beta}{2}(R-r^*)\right]$$
$$-2E_c[1+\alpha(R-r^*)]\exp[-\alpha(R-r^*)]\ . \tag{18}$$

Equation (18) displays the same form for $\phi_{ij}$ as shown in Eq. (16). Comparing the two equations, we find that, for the case of only nearest-neighbor interactions, $B_{ij}=A_i\sqrt{N}$ and $C_{ij}=2E_c$. For a system with more than nearest neighbors interacting, these relationships are not as clearly defined. [One cannot, for instance, use Eq. (18) assuming $N$ is simply an "effective" number of nearest neighbors, as that implies the presence of a unique effective radial cutoff. The presence of different exponents leads to several length scales, and hence more than one effective cutoff.] We will instead take the coefficients in Eq. (16) to be free parameters.

The above discussion of a nearest-neighbor model mirrors the work of Johnson,[25] who performed a similar analysis in the derivation of the analytic embedded-atom potentials. In that case, an exponential form for the pair-pair potential was assumed, resulting in a more complex expression for the embedding energy than the Finnis-Sinclair form. As we do not know the exact form of either the embedding functional or the pair potential, we have chosen a well-known form for the embedding functional and use a pair potential form which allows more flexibility in describing the heteroatomic pair interactions.

For homoatomic pairs, the parameters $\beta_{ii}$ and $r_{ii}^*$ equal the atomic parameters $\beta_i$ and $r_i^*$, respectively. The atomic parameters $A_i$, $\beta_i$, $\xi_j$, $r_i^*$ and the pair-potential parameters $\alpha_{ij}$, $\beta_{ij}$, $r_{ij}^*$, $B_{ij}$, and $C_{ij}$, as well as the electrostatic parameters above are chosen by optimization to a range of structural properties. In particular for aluminum and $\alpha$-alumina, we fit these parameters to the cohesive energies, lattice parameters, and elastic constants of both aluminum metal and $\alpha$-alumina, as well as the surface energies of several of their low-index faces.

The total energy of a set of interacting cations and anions within the ES+EAM model can be simply written as $E_{\mathrm{tot}}=E_{\mathrm{es}}(q,\mathbf{r})+E_{\mathrm{EAM}}(\mathbf{r})$. Forces are given by the appropriate derivatives with resect to Cartesian coordinates of the atomic positions. Consider one such derivative:

$$-f_x=\frac{dE_{\mathrm{tot}}}{dx}=\sum_i\frac{\partial E_{\mathrm{es}}}{\partial q_i}\frac{\partial q_i}{\partial x}+\frac{\partial E_{\mathrm{es}}}{\partial x}+\frac{\partial E_{\mathrm{EAM}}}{\partial x}\ . \tag{19}$$

Because the charges $q_i$ are each chosen to minimize the electrostatic energy, all derivatives $\partial E_{\mathrm{es}}/\partial q_i$ are identically equal. Interchanging the order of summation and differentiation, we can write the term involving derivatives of $q_i$ as

$$\sum_i\frac{\partial E_{\mathrm{es}}}{\partial q_i}\frac{\partial q_i}{\partial x}=\mu\frac{\partial}{\partial x}\sum_i q_i=0\ , \tag{20}$$

since $\sum_i q_i=0$. Thus, no $\partial q/\partial r$ terms appear in the expressions for force and pressure.

## DISCUSSION

Our primary goal in this work was to demonstrate the viability of a model which can simultaneously treat a pure metal and an ionic metal oxide, yielding reasonable calculated values not only for the bulk properties but also the surface energies and expected surface relaxation. For this reason we have chosen the parameters summarized in Table I to optimize the bulk properties of both the fcc aluminum and $\alpha$-alumina crystal structures, as well as reasonable values for two $\alpha$-alumina surfaces. We obtained these parameters by first optimizing the homoatomic aluminum parameters in Table I to the lattice parameters and elastic constants for fcc aluminum. We exclude the electrostatic parameters, which have no effect in bulk fcc aluminum in this model, as all atoms will have zero charge. This was done by using a simplex fit algorithm to minimize the least-squares weighted error between our calculated values and the experimental values of the cohesive energy, pressure, and elastic constants for fcc aluminum.[36–38] Next we optimized the remaining parameters in Table I using the same techniques to mini-

TABLE I. Optimized ES+ potential parameters for aluminum and oxygen.

| | Atomic parameters | | | | | |
|---|---|---|---|---|---|---|
| | $\chi$ (eV) | $J$ (eV) | $\zeta$ (Å$^{-1}$) | $Z$ | $A$ (eV) | $\xi$ |
| Al | 0.000 000 | 10.328 655 | 0.968 438 | 0.746 759 | 0.763 905 | 0.147 699 |
| O | 5.484 763 | 14.035 715 | 2.143 957 | 0.000 000 | 2.116 850 | 1.000 000 |
| | Pair parameters | | | | | |
| | $r^*$ (Å) | $\alpha$ (Å$^{-1}$) | $\beta$ (Å$^{-1}$) | $B$ (eV) | $C$ (eV) | |
| Al-Al | 3.365 875 | 1.767 488 | 2.017 519 | 0.075 016 | 0.159 472 | |
| O-O | 2.005 092 | 8.389 842 | 6.871 329 | 1.693 145 | 1.865 072 | |
| Al-O | 2.358 570 | 4.233 670 | 4.507 976 | 0.154 548 | 0.094 594 | |

mize a least-squares weighted error for our calculated cohesive enrgy, cationic charge, pressures, forces on the nuclei, elastic constants, and unrelaxed surface enrgies for the (0001) and $(10\bar{1}2)$ surfaces of $\alpha$-alumina with experimental values[39–42] and first-principles theoretical results.[43,44] Table II summarizes the results of these fitting procedures, comparing calculated versus experimental structural parameters and elastic constants for fcc aluminum and $\alpha$-alumina. The aluminum results are typical of EAM results for aluminum. The structures are those from Slater,[41] and we can require the model structures to match the experimental crystal structures to within 1%. The value of cationic charge $q_{\mathrm{Al}}$ requires more comment. The experimental result cited is based on analysis of x-ray crystallographic structure factors.[40] Theoretical estimates of the cation charge vary from 1.09 to 3.0.[9,44–47] As the appropriate ionic content of alumina is still an open question in the literature, we have chosen to accept any value for $q_{\mathrm{Al}}$ between the crytallographic result of 1.3 and the formal charge of 3.0 as reasonable. The elastic constants are in excellent agreement with experiment, and compare favorably with results using other empirical ionic models.[48–50]

Manassidis and co-workers[43,44] have recently reported first-principles local-density functional (LDF) theoretical calculations for the (0001), $(10\bar{1}0)$, $(10\bar{1}1)$, $(10\bar{1}2)$, and $(11\bar{2}0)$ surfaces of $\alpha$-alumina. As a test of our method, we have performed equivalent calculations using our empirical ES+ potential for surfaces energies of these low-index faces. These results are summarized in Table III. As in the first-principles results, these are performed for finite thickness stoichiometric slabs, with the surface energy defined as the total energy per cell (with two-dimensional periodic boundary conditions) minus the total energy for the same number of atoms in the crystal, divided by the total area of both surfaces of the slab unit cell. We calculated surface energies both for the unrelaxed surfaces obtained using the crystal structural parameters, and relaxed surfaces obtained by minimization of the total energy of the slab with respect to nuclear coordinates using either a Broyden-Fletcher-Goldfarb-Shanno scheme[51–53] or by simply cooling the system using molecular dynamics. We also compare with the results by Mackrodt and co-workers[48,49] using a pair-potential scheme for the interactions between ions, denoted herein as the interaction model (IM). Simulations using a related ionic scheme have also been reported,[50] with results similar to those reported by Mackrodt and co-workers. As in both the LDF and IM results, we find that relaxation of the surface leads to a marked reduction of the surface energies. We show in Fig. 1 the unrelaxed and relaxed surface energies for all five surfaces studied. We note that our results agree quite closely with the LDF calculations, predicting the same nature and extent of relaxation in these surfaces. As in the LDF and IM results, we find that relaxation changes the energetic ordering of the surfaces.

All of the slabs used in the LDF work are less than 8 Å in thickness. We have also calculated surface energies for thicker slabs and find that except for the $(10\bar{1}0)$ surface, the changes in calculated surface energies are modest and less than 10%. Manassidis and Gillan comment in their work that the small maximum size of their unit cells (20 atoms) leads to an exceptionally thin model slab for the $(10\bar{1}0)$ surface (3 Å) and that they expect larger slabs may lead to substantially different relaxed surface energies. Figure 2 depicts the relaxed and unrelaxed surface energies for this surface as a function of slab thickness.

TABLE II. Structural parameters and elastic constants for fcc aluminum and $\alpha$-alumina.

| | ES+ | Experiment |
|---|---|---|
| | fcc aluminum | |
| $E_c$ (eV/Al) | 3.39 | 3.39[a] |
| $a$ (Å) | 4.05 | 4.05[b] |
| $c_{11}$ (GPa) | 94 | 107[c] |
| $c_{12}$ (GPa) | 77 | 61[c] |
| $c_{44}$ (GPa) | 34 | 28[c] |
| | $\alpha$-alumina | |
| $E_c$ (eV/$Al_2O_3$) | 31.8 | 31.8[d] |
| $q_{\mathrm{Al}}$ ($e$) | 2.9 | 1.3[e] |
| $a$ (Å) | 5.13 | 5.13[f] |
| $u$ | 0.303 | 0.303[f] |
| $v$ | 0.105 | 0.105[f] |
| $c_{11}$ (GPa) | 537 | 497[g] |
| $c_{12}$ (GPa) | 180 | 164[g] |
| $c_{13}$ (GPa) | 106 | 111[g] |
| $c_{33}$ (GPa) | 509 | 498[g] |
| $c_{14}$ (GPa) | −30 | −24[g] |
| $c_{44}$ (GPa) | 130 | 147[g] |
| $c_{66}$ (GPa) | 179 | 167[g] |

[a]Reference 36.
[b]Reference 37.
[c]Reference 38.
[d]Reference 39.
[e]Reference 40.
[f]Reference 41.
[g]Reference 42.

TABLE III. Calculated unrelaxed and relaxed surface energies ($J/m^2$) for (0001), $(10\bar{1}0)$, $(11\bar{2}0)$, $(10\bar{1}2)$, and $(10\bar{1}1)$ surfaces of $\alpha$-alumina. ES+ refers to this work, LDF refers to first-principles local-density functional results (Refs. 43 and 44), and IM refers to interaction model results (Refs. 48 and 49).

| | ES+ | | LDF | | IM | |
|---|---|---|---|---|---|---|
| | Unrelaxed | Relaxed | Unrelaxed | Relaxed | Unrelaxed | Relaxed |
| (0001) | 3.67 | 2.67 | 3.77 | 1.76 | 5.95 | 2.03 |
| $(10\bar{1}0)$ | 3.18 | 1.28 | 3.59 | 1.40 | 6.46 | 2.23 |
| $(10\bar{1}1)$ | 3.22 | 2.13 | 3.64 | 2.55 | 5.58 | 2.52 |
| $(11\bar{2}0)$ | 2.52 | 1.81 | 2.49 | 1.86 | 4.37 | 2.50 |
| $(10\bar{1}2)$ | 2.42 | 1.80 | 2.51 | 1.97 | 3.63 | 2.29 |

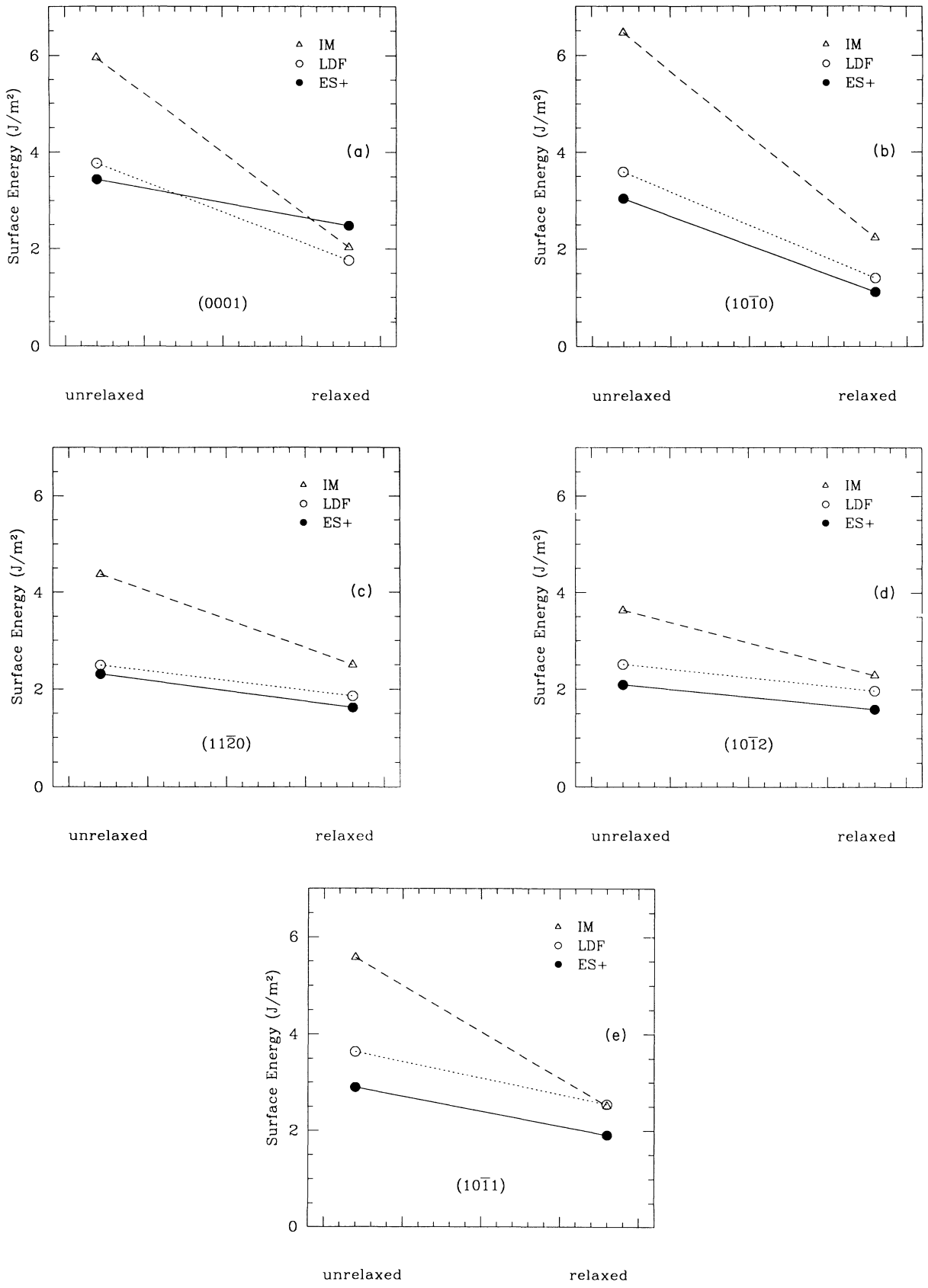


FIG. 1. Unrelaxed and relaxed surface energy for (a) (0001), (b) (10$\bar{1}$0), (c) (11$\bar{2}$0), (d) (10$\bar{1}$2), and (e) (10$\bar{1}$1) surfaces of $\alpha$-alumina, respectively. ES+ refers to this work, LDF refers to local-density functional results (Refs. 43 and 44), and IM refers to the interaction model results (Refs. 48 and 49).

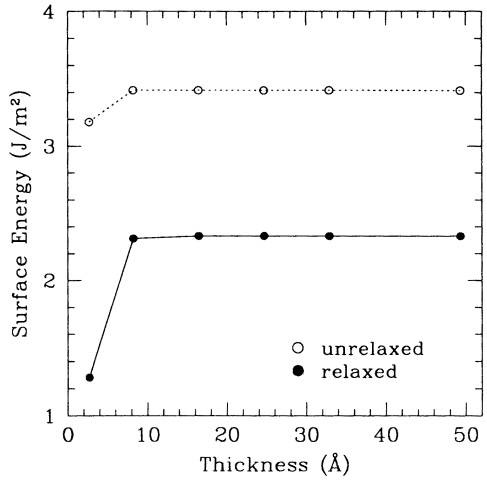


FIG. 2. Calculated values of unrelaxed and relaxed surface energy for $(10\bar{1}0)$ surface of $\alpha$-alumina as a function of slab thickness.

We see that for the thicker films the unrelaxed and relaxed surface energies converge to values of 3.4 and 2.3 $J/m^2$, respectively.

Table IV reports our calculated surface relaxation for the (0001) surface and compares these results with the LDF and IM results. The (0001) basal-plane orientation consists of repeating blocks of two closely spaced lanes of aluminum (with an interplanar separation of 0.56 Å) followed by a plane of oxygens (with an interplanar separation between aluminum and oxygen planes of 0.80 Å). As in the LDF and IM simulations, we terminate the surface with a single plane of aluminum. As Table IV indicates, our results are consistent with both LDF and IM models. Within the ES+ model, the unrelaxed surface has extremely strong forces on the outer layer of aluminum atoms, of the order of 10 nN. These forces are largely the result of unbalanced electrostatic forces. The calculated local charges of the outer layer of aluminum atoms and the next layer of oxygen atoms are 1.55 and −1.38 electron charges, respectively, compared to bulk calculated values of 2.86 and −1.91, respectively. We plot in Fig. 3 the local charge for the cation and anion, both before and after relaxation, as a function of distance from the free surface. We see that with the creation of a (0001) face, a large amount of charge is transferred back to the aluminum at the surface. As a result of the substantial surface relaxation, some of this charge transfer is reversed. After relaxation, the surface Al atoms in the ES+ model are reduced to approximately 75% of their bulk charge, with a similar change occurring in the O atoms just below the surface. Note that this effect is very short ranged: atoms of both species even one layer down from the surface are within a few percent of their bulk charge. Mackrodt has estimated the valence change of the (0001) surface Al and O atoms in alumina to be much smaller (about 7%) based on Hartree-Fock calculations made on a slab with only the top three layers allowed to relax.[54] Because surface relaxations typically extend farther than three layers, we cannot compare the charge relaxation seen in that simulation with the valence changes observed during reconstruction of an unconstrained slab.[43,54]

TABLE IV. Interplanar relaxations for (0001) surface. Element names refer to composition of planes starting with top layer of the surface, and the numbers refer to percentage changes of the interlayer changes relative to the bulk spacings caused by relaxation at the surface. ES+ refers to this work, LDF refers to first-principles local-density functional results (Refs. 43 and 44), and IM refers to interaction model results (Ref. 43).

| | ES+ | LDF | IM |
|---|---|---|---|
| Aluminum | | | |
| | −49 | −86 | −65 |
| Oxygen | | | |
| | +10 | +3 | −5 |
| Aluminum | | | |
| | −48 | −54 | −32 |
| Aluminum | | | |
| | +24 | +25 | +14 |
| Oxygen | | | |

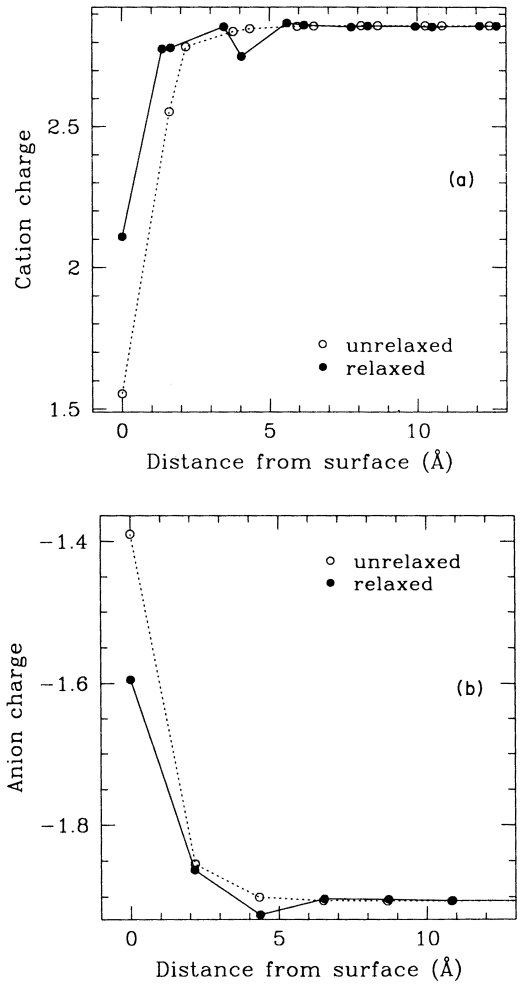


FIG. 3. Cation (a) and anion (b) charge as a function of distance from unrelaxed and relaxed (0001) free surface in $\alpha$-alumina.

## SUMMARY

In summary, we have developed an electrostatic model for metal oxides which calculates both a local atomic charge and the electrostatic potential as a function of nuclear coordinates. We have constructed an overall empirical potential that merges the electrostatic potential with an embedded-atom method potential, which we refer to as the electrostatic-plus model. We have shown this potential to be effective in describing the cohesive, structural, and elastic properties of both fcc aluminum and $\alpha$-alumina. Simulations of low-index faces of $\alpha$-alumina are in good agreement with the results of first-principles LDF simulations. The combination of agreement in both surface energies and relaxations leads us to conclude that the ES+model we propose includes the basic physics and chemistry necessary to describe these surfaces.

## ACKNOWLEDGMENTS

This work was supported by the U.S. Office of Naval Research both through the U.S. Naval Research Laboratory and directly from the Chemistry and Materials Divisions of ONR. F.H.S. acknowledges support through the NRC-NRL Postdoctoral Associateship Program.

[1]R. P. Iczkowsky and J. L. Margrave, J. Am. Chem. Soc. **83**, 3547 (1961).
[2]R. G. Parr, R. A. Donnelly, M. Levy, and W. E. J. Palke, J. Chem. Phys. **68**, 3801 (1978).
[3]R. G. Parr and R. G. Pearson, J. Am. Chem. Soc. **105**, 7512 (1983).
[4]W. J. Mortier, K. van Genechten, and J. Gasteiger, J. Am. Chem. Soc. **107**, 829 (1985).
[5]W. J. Mortier, S. K. Gosh, and S. Shankar, J. Am. Chem. Soc. **108**, 4315 (1986).
[6]A. K. Rappé and W. A. Goddard, J. Phys. Chem. **95**, 3358 (1991).
[7]G. J. Dienes, D. O. Welch, C. R. Fischer, R. D. Hatcher, O. Lazareth, and M. Samberg, Phys. Rev. B **11**, 3060 (1975).
[8]C. R. A. Catlow, R. James, W. C. Mackrodt, and R. F. Stewart, Phys. Rev. B **25**, 1006 (1982).
[9]J. D. Gale, C. R. A. Catlow, and W. C. Mackrodt, Modell. Simul. Mater. Sci. Eng. **1**, 63 (1992).
[10]F. H. Streitz and J. W. Mintmire (unpublished).
[11]N. Rosen, Phys. Rev. **38**, 255 (1931).
[12]C. C. J. Roothan, J. Chem. Phys. **19**, 1445 (1951).
[13]S. W. de Leeuw, J. W. Perram, and E. R. Smith, Proc. R. Soc. London Ser. A **373**, 27 (1980).
[14]E. R. Smith, Proc. R. Soc. London Ser. A **375**, 475 (1980).
[15]D. E. Parry, Surf. Sci. **49**, 433 (1975).
[16]J. Hautman and M. L. Klein, Mol. Phys. **75**, 379 (1992).
[17]J. W. Mintmire, Ph.D. dissertation, University of Florida, 1980.
[18]D. M. Heyes, Surf. Sci. Lett. **293**, L857 (1993).
[19]F. H. Streitz and J. W. Mintmire, J. Adhesion Sci. Technol. **8**, 853 (1994).
[20]F. H. Streitz and J. W. Mintmire, in *Interface Control of Electrical, Chemical, and Mechanical Properties,* edited by S. P. Murarka, K. Rose, T. Ohmi, and T. Seidel, MRS Symposia Proceedings No. 318 (Materials Research Society, Pittsburgh, 1994), p. 679.
[21]M.S. Daw and M. I. Baskes, Phys. Rev. Lett. **50**, 1285 (1983).
[22]M. S. Daw and M. I. Baskes, Phys. Rev. B **29**, 6443 (1984).
[23]S. M. Foiles, M. I. Baskes, and M. S. Daw, Phys. Rev. B **33**, 7983 (1986).
[24]M. W. Finnis and J. E. Sinclair, Philos. Mag. A **50**, 45 (1984).
[25]R. A. Johnson, Phys. Rev. B **37**, 3924 (1988).
[26]R. A. Johnson, Phys. Rev. B **39**, 12 554 (1989).
[27]G. C. Abell, Phys. Rev. B **31**, 6184 (1985).
[28]J. Tersoff, Phys. Rev. Lett. **61**, 2879 (1988); **56**, 632 (1986).
[29]D. W. Brenner, Phys. Rev. B **42**, 9458 (1990).
[30]D. G. Pettifor, Phys. Rev. Lett. **63**, 2480 (1989).
[31]F. H. Stillinger and T. A. Weber, Phys. Rev. B **31**, 5262 (1985).
[32]J. H. Rose, J. Ferrante, and J. R. Smith, Phys. Rev. Lett. **47**, 675 (1981).
[33]J. Ferrante and J. R. Smith, Phys. Rev. B **31**, 3427 (1985).
[34]J. R. Smith, H. Schlosser, W. Leaf, J. Ferrante, and J. H. Rose, Phys. Rev. A **39**, 514 (1989).
[35]J. Ferrante, H. Schlosser, and J. R. Smith, Phys. Rev. A **43**, 3487 (1991).
[36]C. Kittel, *Introduction to Solid State Physics,* 5th ed. (Wiley, New York, 1976).
[37]N. W. Ashcroft and N. D. Mermin, *Solid State Physics* (Saunders, Philadelphia, 1976).
[38]P. Ho and A. L. Ruoff, J. Appl. Phys. **40**, 3 (1969).
[39]*CRC Handbook of Chemistry and Physics,* 67th ed. (CRC, Boca Raton, FL, 1983).
[40]J. Lewis, D. Schwarzenbach, and H. D. Flack, Acta Crystallogr. Sec. A **38**, 733 (1982).
[41]J. C. Slater, *Symmetry and Energy Bands in Crystals* (Dover, New York, 1972).
[42]J. B. Wachtman, Jr., W. E. Tefft, D. G. Lam, and R. P. Stinchfield, J. Res. Natl. Bur. Stand. **64A**, 213 (1960); J. B. Wachtman, Jr., in *Mechanical and Thermal Properties of Ceramics,* edited by J. B. Wachtman, Jr. (NBS, Washington, 1969), pp. 139–188.
[43]I. Manassidis, A. DeVita, and M. J. Gillan, Surf. Sci. Lett. **285**, L517 (1993).
[44]I. Manassidis and M. J. Gillan, J. Am. Ceram. Soc. **77**, 335 (1994).
[45]M. Causa, R. Dovesi, C. Roetti, E. Kotomin, and V. R. Saunders, Chem. Phys. Lett. **140**, 120 (1987).
[46]L. Salasco, R. Dovesi, R. Orlando, M. Causa, and V. R. Saunders, Mol. Phys. **72**, 267 (1991).
[47]C. Sousa, F. Illas, and G. Pacchioni, J. Chem. Phys. **99**, 6818 (1993).
[48]W.C. Mackrodt, R. J. Davey, S. N. Black, and R. Docherty, J. Cryst. Growth **80**, 441 (1980).
[49]W. C. Mackrodt, J. Chem. Soc. Faraday Trans. II **85**, 541 (1989).
[50]S. Blonski and M. Garofalini, Surf. Sci. **295**, 263 (1993).
[51]R. Fletcher, *Practical Methods of Optimization* (Wiley, Chichester, 1980).
[52]J. E. Dennis, Jr. and R. B. Schnabel, *Numerical Methods for Unconstrained Optimizations and Nonlinear Equations* (Prentice-Hall, Englewood Cliffs, NJ, 1983).
[53]J. D. Head and M. C. Zerner, Chem. Phys. Lett. **122**, 264 (1985).
[54]W. C. Mackrodt, Phil. Trans. R. Soc. London Ser. A **341**, 293 (1992).